

# Controlling atomic spin-mixing via multiphoton transitions in a cavity

Ming Xue,<sup>1,2,\*</sup> Xiangliang Li,<sup>3</sup> Wenhao Ye,<sup>4</sup> Jun-Jie Chen,<sup>5</sup> Zhi-Fang Xu,<sup>6,†</sup> and Li You<sup>3,4,‡</sup>

<sup>1</sup>College of Physics, Nanjing University of Aeronautics and Astronautics, Nanjing 211106, China

<sup>2</sup>Key Laboratory of Aerospace Information Materials and Physics (NUAA), MIIT, Nanjing 211106, China

<sup>3</sup>Beijing Academy of Quantum Information Sciences, Xibeiwang East Road, Beijing 100193, China

<sup>4</sup>State Key Laboratory of Low Dimensional Quantum Physics,

Department of Physics, Tsinghua University, Beijing 100084, China

<sup>5</sup>Equity Derivatives Business Line, CITIC Securities, Liangmaqiao Road, Beijing 100026, China

<sup>6</sup>Shenzhen Institute for Quantum Science and Engineering and Department of Physics,

Southern University of Science and Technology, Shenzhen 518055, China

We propose to control spin-mixing dynamics in a gas of spinor atoms, via the combination of two off-resonant Raman transition pathways, enabled by a common cavity mode and a bichromatic pump laser. The mixing rate, which is proportional to the synthesized spin-exchange interaction strength, and the effective atomic quadratic Zeeman shift (QZS), can both be tuned by changing the pump laser parameters. Quench and driving dynamics of the atomic collective spin are shown to be controllable on a faster time scale than in existing experiments based on inherent spin-exchange collision interactions. The results we present open a promising avenue for exploring spin-mixing physics of atomic ensembles accessible in current experiments.

## I. INTRODUCTION

Establishing quantum entanglement between two parties is crucial to quantum technology [1, 2]. A direct approach for entanglement generation is based on coherent interaction between parties. To manipulate and protect quantum entanglement in a quantum many-body system, strong and precisely controllable quantum interaction is required. Quantum phases with different entanglement properties can be realized by tuning relative strengths of competing interactions [3].

Between spinful atoms, spin-exchange interaction naturally arises when binary collision strengths differ for different total spin channels [4, 5]. Coherent quantum spin-mixing dynamics, modeled by contact spin-exchange interaction between pairs of atoms, have been observed for spinor Bose-Einstein condensate (BEC) in all-optical trap experiments, using <sup>87</sup>Rb, <sup>23</sup>Na, <sup>7</sup>Li atoms [6–11], as well as their mixtures [12–14]. The resulting collective population oscillations among different spin states, enable the exploration of many-body physics related to spin degrees of freedom, e.g., spin squeezing [15–18], generation of metrologically meaningful entangled states [19–23], and in probing nonequilibrium dynamics [24–29]. Any endeavor to establish tunable two-body interaction is desirable for ground-state atoms in a condensate, where inherent atomic spin-exchange interaction is nominally weak [8–11].

Varying the density of particles could simply tune atomic interaction strength versus single-particle energy [30]. More elaborate techniques like Feshbach resonance (FR) achieves the same at constant density [31], by

tuning the scattering energy between two atoms through a nearby closed-channel molecular bound state [32–35], which in some limiting cases can be viewed as inducing atom-atom interactions by coupling off-resonantly to their bound molecular state. Such a picture extrapolates smoothly to the scenario of indirect interaction mediated by a quantum channel, or more generally any intermediate bosonic quantum object. The physical constituent of the channel can be an electromagnetic field mode in a cavity or photonic crystal [36–43], vibrational phonons in trapped ions [44–46] or opto(sp)in-mechanical hybrid system [47, 48], and atoms with dipole-dipole interactions limited to excited Rydberg state manifold [49–55].

Here in this work, we present a simple but efficient scheme for controlling spin-mixing dynamics in spinor atomic gases using only optical fields. Extending earlier studies [41, 42, 56], we show that by using two  $\sigma$ -polarized laser fields in an atom-cavity system, the effective spin-exchange interaction between ground-state atoms and the effective atomic quadratic Zeeman shift (QZS) become tunable without requiring more complicated setups. Besides synthesized spin-exchange interaction in spin-1 atoms as previously studied [41, 42, 56], the ability to tune QZS in the present scheme provides a critical ingredient for realizing a rich variety of quantum phases [57, 58] and for related quantum metrological applications of spinor atoms [19–22, 59]. The effective QZS can be easily tuned to compete with photon-mediated effective interaction by simply varying the differential laser detuning, resulting in the formation of different quantum phases as well as for providing faster controlled dynamics [22, 57, 58]. Thus our work goes beyond that of the analogously synthesized interactions in spin-1 atomic systems of earlier studies [41, 42, 56], where only linear Zeeman shifts in external magnetic fields were considered and QZSs were not tunable without additional dressing laser or microwave fields [41, 56]. By facilitating easy tuning of both the effective spin-exchange strength and QZS,

\* mxue@nuaa.edu.cn

† xuzf@sustech.edu.cn

‡ lyou@tsinghua.edu.cn

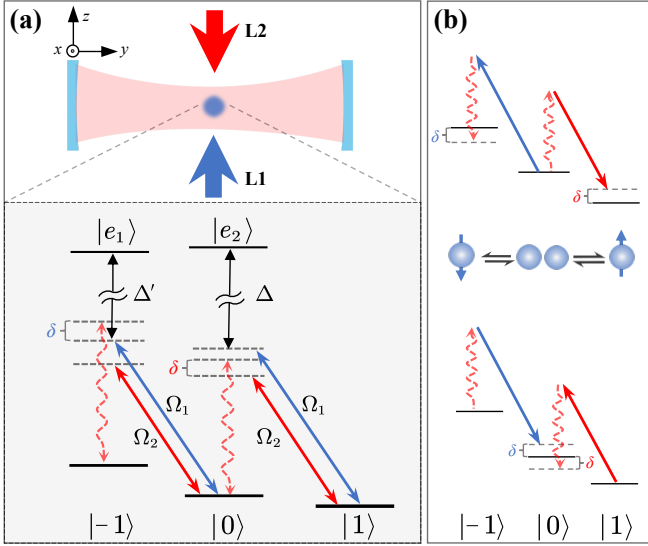


FIG. 1. (a) Atoms inside an optical cavity are pumped by two  $\sigma_-$ -polarized lasers with frequencies  $\omega_1, \omega_2$  and Rabi frequencies  $\Omega_1, \Omega_2$  from side, denoted as L1 (blue) and L2 (red solid lines), respectively. Spin-1 atomic ground states ( $|0\rangle, |-1\rangle$ ) are coupled to two excited states  $|e_1\rangle, |e_2\rangle$  by a single cavity mode (red-wavy lines) with frequency  $\omega_c$  and coupling strength  $g_{i=1,2}$ . Cavity axis is along the  $y$ -direction with polarization axis along  $z$ , the direction of external magnetic field  $B_z$ . (b) Taking  $\omega_1 - \omega_2 = 2q$ , the two four-photon Raman transition pathways illustrated give rise to resonant atomic spin-exchange.

our approach can be adapted to systems inside a significant bias magnetic field, while maintaining the desired interaction and the consequent spin-mixing dynamics.

## II. MODEL AND HAMILTONIAN

Our scheme is illustrated intuitively as in Fig. 1 for a cloud of spin-1 atomic gas or BEC tightly trapped inside an optical cavity. To simplify our discussion, atom-light coupling is assumed spatially uniform, which could be achieved by selective loading of atoms into a spatial lattice or alternatively by using a ring cavity [56, 60, 61]. Atoms are pumped by two external  $\sigma_-$ -polarized lasers (labeled as L1 and L2 with respective frequencies  $\omega_1$  and  $\omega_2$ ) from the side and also are coupled to a single cavity mode (with frequency  $\omega_c$ ). The atomic level diagram contains two excited states  $|e_1\rangle$  and  $|e_2\rangle$ , e.g., the  $5P_{1/2}$  or  $5P_{3/2}$  states for  $^{87}\text{Rb}$  atoms [61]. In the lower panel of Fig. 1 (a), L1 and L2 induce  $\sigma$ -transitions  $|0\rangle \leftrightarrow |e_1\rangle$  and  $|1\rangle \leftrightarrow |e_2\rangle$  with coupling strengths  $\tilde{\Omega}_{i=1,2}$  and  $\Omega_{i=1,2}$  ( $\tilde{\Omega}_i = \Omega_i$  is assumed), and the cavity field (wavy line) couples  $\pi$ -transitions  $|0\rangle \leftrightarrow |e_2\rangle$  and  $|-1\rangle \leftrightarrow |e_1\rangle$  with strengths  $g_1$  and  $g_2$ , respectively.

Spinor BEC of  $F = 1$  ground state atoms, e.g.,  $^{23}\text{Na}$  or  $^{87}\text{Rb}$  atoms with anti-ferromagnetic or ferromagnetic spin-exchange interactions have been studied

extensively [10, 22, 62–65]. Under single-mode approximation [5, 9, 16, 18, 66–68] for the spin component density profiles, atomic spin-mixing dynamics in a magnetic field as depicted in Fig. 1 is governed by the Hamiltonian  $\hat{H} = \hat{H}_0 + \hat{H}_B + \omega_c \hat{c}^\dagger \hat{c} + \hat{H}_{\text{AL}}$  ( $\hbar = 1$ ) [5, 66], with  $\hat{H}_0 = (c/2N)[(\hat{N}_1 - \hat{N}_{-1})^2 + (2\hat{N}_0 - 1)(\hat{N}_1 + \hat{N}_{-1}) + 2(\hat{a}_1^\dagger \hat{a}_{-1}^\dagger \hat{a}_0 \hat{a}_0 + \text{h.c.})]$  resulting from inherent two-body  $s$ -wave spin-exchange at rate  $c$  and  $N$  the total number of atoms.  $\hat{a}_{m=0,\pm 1}$  denotes annihilation operator for condensed atoms in spin component  $|F = 1, m\rangle$  and  $\hat{N}_m = \hat{a}_m^\dagger \hat{a}_m$  the corresponding number operator. The Zeeman term inside a magnetic field is given by  $\hat{H}_B = -p\hat{F}_z + q(\hat{N}_1 + \hat{N}_{-1})$  (wherein  $\hat{F}_z \equiv \hat{N}_1 - \hat{N}_{-1}$ ), with  $p$  the single-atom linear Zeeman shift and  $q$  the QZS which competes with spin exchange interaction ( $\propto c$ ) to govern system spin-mixing dynamics. The differential laser frequency shift is set as  $\omega_1 - \omega_2 = 2q$ , exactly equal to the two-atom energy deficit if spin-exchange is to occur on resonance. This is a necessary condition for efficient spin-mixing, especially when the bias magnetic field induced QZS is large and the energy matching condition is destroyed for spin-exchange collision [41, 42, 56].  $\omega_c \hat{c}^\dagger \hat{c}$  is the free cavity-photon Hamiltonian and the atom-light interaction Hamiltonian  $\hat{H}_{\text{AL}}$  describes the multiphoton transitions shown in the lower panel of Fig. 1 (a).

In a typical ultracold  $^{87}\text{Rb}$  atom experiment, one finds  $|c| \lesssim (2\pi)10\text{Hz}$  [8, 16, 22, 26]. Assuming an applied magnetic field ranging from tens to hundreds of Gauss, the induced Zeeman effects satisfy:  $p \gg q \gg |c|$ . Therefore, two-body collision induced spin-mixing processes in  $\hat{H}_0$  is highly suppressed by the large energy mismatch between spin-exchanged states.

The atom-light interaction Hamiltonian  $\hat{H}_{\text{AL}}$  under rotating-wave approximation becomes [69, 70]

$$\hat{H}_1 = \sum_{j=1}^N \left[ \left( \Omega_1 e^{i\varphi} e^{-i\Delta t} + \Omega_2 e^{-i(\Delta+2q)t} \right) |1\rangle_j \langle e_2| + \left( \tilde{\Omega}_1 e^{i\varphi} e^{-i\Delta' t} + \tilde{\Omega}_2 e^{-i(\Delta'+2q)t} \right) |0\rangle_j \langle e_1| + g_1 \hat{c}^\dagger e^{-i(\Delta+2q-\delta)t} |0\rangle_j \langle e_2| + g_2 \hat{c}^\dagger e^{-i(\Delta'-\delta)t} |-1\rangle_j \langle e_1| + \text{h.c.} \right], \quad (1)$$

where  $\varphi$  is the initial phase difference between the two lasers ( $\varphi = 0$  hereafter).  $\Delta$  ( $\Delta'$ ) denotes detuning of L1 from the transition  $|1\rangle \leftrightarrow |e_2\rangle$  ( $|0\rangle \leftrightarrow |e_1\rangle$ ) which can take values in the range of GHz and even THz between ground state manifold and alkali atom D-line transitions in the optical range [71], and the detunings for the L2 couplings are  $\Delta + 2q$  and  $\Delta' + 2q$  respectively. With suitably locked cavity  $\omega_c$ , we denote  $2q - \delta$  ( $\delta$ ) as the detuning for the two-photon Raman transition pathways between  $|0\rangle$  and  $|1\rangle$  ( $|-1\rangle$ ), with L1 (L2) and the cavity field shown respectively in the lower panel of Fig. 1 (a).

*Effective Hamiltonian.*—When the detunings between optical fields and atomic transitions are large, i.e.,  $|g_{1,2}|, |\Omega_{1,2}|, |\tilde{\Omega}_{1,2}| \ll \Delta^{(i)}, \Delta^{(i)} + 2q, \Delta + 2q - \delta, \Delta' - \delta,$

one can neglect atomic spontaneous emission and safely eliminate the excited states  $|e_1\rangle$  and  $|e_2\rangle$  to obtain the Hamiltonian projected onto the spin-1 atomic ground state manifold [40, 41, 69],

$$\hat{H}_2 = \{[\eta_1 e^{i(\delta-2q)t} + \eta_2 e^{i\delta t}]\hat{a}_0^\dagger \hat{a}_1 \hat{c}^\dagger + [\tilde{\eta}_1 e^{i\delta t} + \tilde{\eta}_2 e^{i(2q+\delta)t}]\hat{a}_{-1}^\dagger \hat{a}_0 \hat{c}^\dagger + \text{h.c.}\}, \quad (2)$$

where the two-photon Raman coupling strengths satisfy  $\eta_1 \approx \tilde{\eta}_1$ ,  $\eta_2 \approx \tilde{\eta}_2$ , after ac Stark shifts induced by light fields are neglected for the three ground-state levels [70].

Since the parameters  $2q \pm \delta$  and  $\delta$  are larger than  $N|\eta_{1,2}|$  in typical experiments, the cavity-assisted Raman coupling between different ground states are far off-resonant, except for the four-photon resonance pathways (presented in Fig. 1(b)) accompanied by two atom spin-exchange that conserves the total z-component angular momentum  $|0\rangle + |0\rangle \rightleftharpoons |1\rangle + |-1\rangle$  [8]. We take  $\delta = 3q/2$ , the Hamiltonian  $\hat{H}_2$  in Eq. (2) then reduces to be time-periodic with fundamental frequency  $2q - \delta = q/2$ . Since  $q/2$  is large compared to the magnitudes of matrix elements of the Hamiltonian, a time-independent effective Hamiltonian can be derived by adopting the high-frequency expansion [70, 72]. The Raman transition pathways (L1/L2 plus cavity mode in Fig. 1) with large two-photon detunings would only virtually excite the cavity mode if one starts from a cavity in vacuum state [40, 73]. The condition of  $\delta = q$  is avoided in order to circumvent simultaneous cavity-photon-pair-creation ( $\hat{c}^\dagger \hat{c}^\dagger$ -term) in the four-photon resonance, although such processes can be used to generate multiphoton pulses [74]. Therefore we substitute the cavity mode operators by  $\langle \hat{c}^\dagger \rangle = 1$  approximately, and neglect other cavity operators that shall remain negligibly small. Finally, we obtain the time-independent effective Hamiltonian [70],

$$\hat{H}_{\text{eff}} = (\tilde{c}/N)(\hat{a}_1^\dagger \hat{a}_{-1}^\dagger \hat{a}_0 \hat{a}_0 + \hat{a}_0^\dagger \hat{a}_0^\dagger \hat{a}_1 \hat{a}_{-1}) - \tilde{q}_0 \hat{N}_{-1} \hat{N}_0, \quad (3)$$

with effective spin-mixing rate coefficient  $\tilde{c} = -2\sqrt{3}N\eta^2/(3q)$  and  $\tilde{q}_0 \sim \mathcal{O}(\tilde{c}/N)$  when  $\eta^2 = \eta_1^2 = \eta_2^2/3$  are taken. We have neglected a minute quadratic Zeeman term  $-\tilde{q}_0 \hat{N}_0$  in deriving Eq. (3) as detailed in the supplemental material [70], since  $|\tilde{q}_0| \ll |\tilde{c}|$  as a result of  $N \gg 1$  implies spin-mixing dynamics is hardly modified. The spin-mixing term ( $\hat{a}_1^\dagger \hat{a}_{-1}^\dagger \hat{a}_0 \hat{a}_0 + \text{h.c.}$ ) in the effective Hamiltonian Eq. (3) thus is engineered based on the intuitive two off-resonant Raman pathways, as depicted in Fig. 1(b). The remaining density interaction is proportional to  $\hat{N}_{-1} \hat{N}_0$ , which can be regarded as a  $\hat{N}_{-1}$ -dependent QZS and may be neglected if the intermediate states have vanishing population in  $|-1\rangle$  during spin-mixing.

*Tunability.*—The effective cavity-mediated spin-mixing rate coefficient per atom  $|\tilde{c}|/N \propto \eta^2/q$  is directly determined by the intensities and detunings of the pump laser fields, while the single-atom QZS ( $q$ ) remain tunable as in previous implementation by changing the applied magnetic or near-resonant microwave dressing

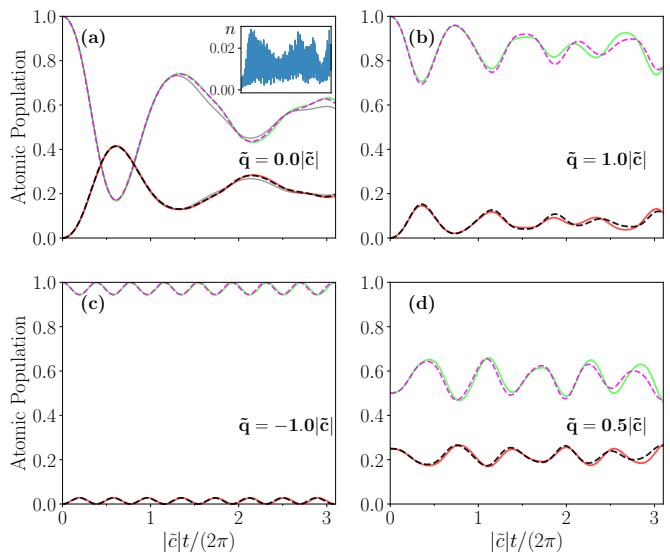


FIG. 2. Spin state atomic populations during quench- $\tilde{q}$  dynamics. Solid (dashed) lines denote simulations with  $\hat{H}_2$  ( $\hat{H}_{\text{eff}}$ ), shown in cyan-solid (magenta-dashed) and red-solid (black-dashed) lines for  $n_0(t)$  and  $n_1(t)$ , respectively. (a-c) for evolution from initial state  $|\Psi_0\rangle = |0, N, 0\rangle \otimes |0\rangle_c$  with effective QZS  $\tilde{q} = 0|\tilde{c}|$ ,  $1.0|\tilde{c}|$ , and  $-1.0|\tilde{c}|$ , respectively. Grey-solid lines in (a) are results with cavity dissipation  $\kappa = 2|\tilde{c}|$  included, and the inset of (a) shows photon population  $n(t)$  of the cavity mode during quench- $\tilde{q}$  dynamics. (d) for  $|\Psi_0\rangle = |N/4, N/2, N/4\rangle \otimes |0\rangle_c$  and  $\tilde{q} = 0.5|\tilde{c}|$ . Other parameters used for numerical simulation are  $N = 20$  and  $q = 6N\eta$ .

fields [16, 75]. These two key parameters governing atomic spin-mixing dynamics are therefore tunable experimentally. The sign of  $\tilde{c}$  could also change to be positive, *i.e.*, becoming antiferromagnetic-like when the two Raman couplings assume an alternative configuration of detunings. This could be used to simulate dynamics of anti-ferromagnetically interacting spin-1 BEC [76–78], in a ferromagnetic one like  $^{87}\text{Rb}$  atoms.

In pioneering experimental studies [18, 22, 75, 78], microwave dressing fields are implemented to augment the effective tuning of QZS from positive to negative, however with tunable range limited by the available power of microwave field. In the scheme we present, effective control of QZS can be directly accomplished, without requiring microwave or optical dressing, but by a slight detuning from the four-photon resonance in Fig. 1(b), namely by taking the differential laser frequency  $\omega_1 - \omega_2 = 2(q - \tilde{q})$ . An effective quadratic Zeeman term  $\mathcal{H}_{\text{QZS}} = -\tilde{q}\hat{N}_0$  in addition to the effective Hamiltonian  $\hat{H}_{\text{eff}}$  in Eq. (3) would emerge. The deviation of  $2\tilde{q}$  is so small ( $|\tilde{q}| \ll q$ ) that it hardly modifies the effective spin-mixing rate coefficient  $\tilde{c}$ , but the magnitude of  $\tilde{q}$  can be easily controlled to be on the same order of  $|\tilde{c}|$ , *i.e.*  $\tilde{q} \sim |\tilde{c}|$ . This tunable effective QZS constitutes a key contribution of this work which complements the synthesized spin-exchange interaction already discussed [41, 42, 56]. It will enable the realizations of different quantum phases as well as flex-

ible fast dynamics control in spinor atomic BEC for a variety of research topics [15, 22, 26, 79].

Futhermore, the two pump laser beams L1 and L2 in Fig. 1 can be derived from a single laser by an acousto-optic modulator (AOM). Experimentally the difference between  $\omega_1/2\pi$  and  $\omega_2/2\pi$  can be well controlled to a high precision at the order of one Hertz. Therefore the frequency difference  $\omega_1 - \omega_2 = 2q$  ( $\sim$  MHz) between L1 and L2 and the effective QZS  $\tilde{q}$  ( $\sim$  kHz) can both be precisely tuned.

For estimation of parameters and numerical simulations, we use  $^{87}\text{Rb}$  atoms with  $|c| \lesssim (2\pi)10\text{ Hz}$  for  $N \in [10^3, 10^5]$  as in current BEC experiments [18–23], the linear and quadratic Zeeman shifts at bias magnetic field  $B_z$  are given by  $(p, q) = 2\pi(0.70 B_z \text{ MHz/G}, 71.6 B_z^2 \text{ Hz/G}^2)$  [22]. At a high  $B_z = 80\text{ G}$ ,  $(p, q) \approx 2\pi(5.6, 0.46)\text{ MHz}$ , thus one can safely neglect the inherent spin-exchange interaction ( $\propto c$ ) as  $q \gg |c|$ , and spin-mixing becomes highly suppressed by the energy mismatch  $q$  per atom. For a cloud of  $N = 20$  atoms inside an optical cavity, we can take  $g = (2\pi)1.0\text{ MHz}$  [37, 56, 61, 80–82], assume  $g_1 = g_2 \equiv g$  and the Rabi frequencies for the two pump lasers are  $\Omega_1 = \Omega_2 \equiv \Omega = (2\pi)40\text{ MHz}$ , the detunings for the two lasers from  $^{87}\text{Rb}$  atom D-line transition are taken respectively as  $\Delta \approx \Delta' \approx (2\pi)21\text{ GHz}$  [56]. The two-photon Raman coupling strength then reduces to  $\eta \approx 2g\Omega/\Delta \approx (2\pi)3.8\text{ kHz}$ , and the effective spin-mixing rate becomes  $|\tilde{c}| \approx (2\pi)730\text{ Hz}$ , which is many orders of magnitude larger than  $|c|$  from inherent spin-exchange collisions.

### III. NUMERICAL SIMULATIONS

We now confirm the validity of  $\hat{H}_{\text{eff}}$  in Eq. (3) with a tunable effective QZS (*i.e.*  $\tilde{q}$ ) by numerically simulating the quench- $\tilde{q}$  dynamics following earlier experimental protocols [15, 20]. In the Fock state representation, with atom state  $|\psi\rangle = |N_1, N_0, N_{-1}\rangle$  and the cavity state  $|n\rangle_c$ , the complete basis state for the system becomes  $|\Psi\rangle = |\psi\rangle \otimes |n\rangle_c$  specified by  $N_1, N_0, N_{-1}$ , and  $n$ . Assuming atoms initially reside in the polar state  $|\psi_0\rangle = |0, N, 0\rangle$  with zero magnetization, which is easy to prepare experimentally [18, 22], and the cavity is empty in vacuum state  $|0\rangle_c$ , the atomic population  $n_m(t) = \langle \hat{N}_m \rangle / N$  ( $m = 0, \pm 1$ ) is simulated by evolving the initial state  $|\Psi_0\rangle = |\psi_0\rangle \otimes |0\rangle_c$  under both  $\hat{H}_2(t)$  in Eq. (2) and the effective Hamiltonian  $\hat{H}_{\text{eff}}$  in Eq. (3). The two results of quench- $\tilde{q}$  dynamics are compared in Fig. 2. In Fig. 2 (a), with initial atomic polar state, the effective Hamiltonian  $\hat{H}_{\text{eff}}$  is found to work quite well over an extended time scale with respect to the characteristic spin-mixing time scale  $1/|\tilde{c}|$ . The inset of Fig. 2 (a) shows that population of the cavity mode remains negligibly small ( $n \ll 1$ ) during the time evolution, supporting our assumption that cavity mode is only virtually excited and thus our scheme is found to be immune to

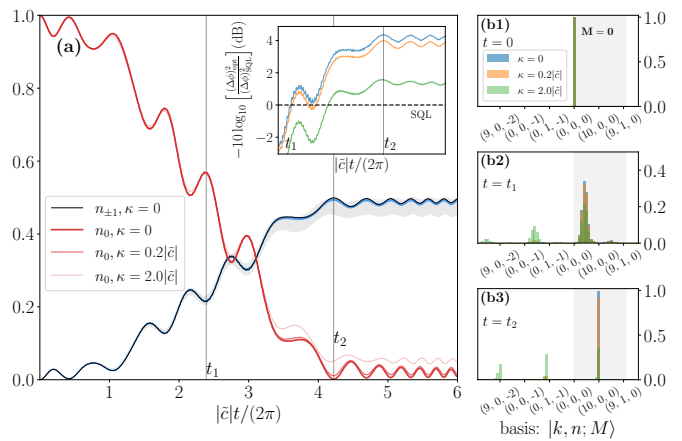


FIG. 3. (a) Adiabatic preparation of atomic twin-Fock state from a linear- $\tilde{q}$  driving starting with an initial polar state  $|N_1, N_0, N_{-1}\rangle = |0, N, 0\rangle$ , of zero magnetization  $M = 0$ . Red- and black-solid lines denote  $n_0$  and  $n_{\pm 1}$  defined in the main text (for  $\kappa = 0$ ), respectively. The shaded area, with upper  $[n_{-1}(t)]$  and lower  $[n_1(t)]$  borderlines surrounding  $n_{\pm 1}$  at  $\kappa = 0$  (black solid line), measures the deviation from  $M = 0$  [ $n_1 = n_{-1}$ ] due to photon loss at rate  $\kappa = 0.2|\tilde{c}|$  (blue shaded) or  $2.0|\tilde{c}|$  (gray shaded), respectively. Inset: metrology gain of optimal phase sensitivity  $[(\Delta\phi)_{\text{opt}}]$  beyond SQL  $[(\Delta\phi)_{\text{SQL}}]$  (dashed line). (b1-b3) The probability distributions of cavity-atom state  $\rho(t)$  in the Fock basis  $|k, n; M\rangle$  at different time  $t = 0, t_1$ , and  $t_2$  [labeled by gray vertical lines in (a)] respectively.  $N = 20$ ,  $q = 6N\eta$ , and the Hilbert space is truncated at  $|M| \leq 2$  with  $\max n = 1$ .

photon loss. By adjusting the laser frequency difference between L1 and L2, we effectively tune the QZS by  $\tilde{q}$ . Figures 2 (b) and (c) show evolutions from the same state  $|0, N, 0\rangle \otimes |0\rangle_c$  but at different effective QZS  $\tilde{q} = \pm|\tilde{c}|$ . Comparisons are also performed for a different initial state  $|\Psi_0\rangle = |N/4, N/2, N/4\rangle \otimes |0\rangle_c$  in Fig. 2 (d) whose results again support the validity of the effective Hamiltonian in Eq. (3).

The effects of photon loss from cavity can be included by employing master equation for the complete cavity-atom state  $\rho$ ,

$$\partial_t \rho(t) = -i[\hat{H}_2(t), \rho] + (\kappa/2)\mathcal{D}(\hat{c}, \rho), \quad (4)$$

where the Lindblad term  $\mathcal{D}(\hat{c}, \rho) = 2\hat{c}\rho\hat{c}^\dagger - \hat{c}^\dagger\hat{c}\rho - \rho\hat{c}^\dagger\hat{c}$  describes dissipative processes associated with cavity loss at rate  $\kappa$ . We can use an ultranarrow-band optical cavity with  $\kappa/(2\pi)$  at the order of  $\sim$  kHz [83–85], hence we choose  $\kappa/|\tilde{c}| = 0, 0.2, 2.0$  for the following simulations at  $N = 20$ . We find that evolutions of atomic populations are hardly modified when cavity dissipations are included as shown in Fig. 2 (a) by grey solid lines ( $\kappa = 2|\tilde{c}|$ ).

To emphasize the utility of controlling both  $\tilde{c}$  and  $\tilde{q}$  in the present scheme, we simulate a dynamic driving- $\tilde{q}$  protocol as shown in the inset of Fig. 3, which is implemented here for adiabatic preparation of metrologically useful quantum entangled states [22, 23]. The effective QZS  $\tilde{q}$  is swept linearly by scanning frequency difference of the two pump lasers, from polar to twin-Fock

phases of the instantaneous effective Hamiltonian. Figure 3 (a) shows the atomic population transfer from  $|0\rangle$  to the spin  $|\pm 1\rangle$  states largely follows the driving- $\tilde{q}$ , and almost perfectly prepares the desired twin-Fock state at the moment of  $t = t_2$  as clearly revealed by the state distribution in the Fock basis  $|k, n; M\rangle$  in Fig. 3 (b3). A short hand for the basis state is now indexed according to  $|k, n; M\rangle \equiv |N_1, N_0, N_{-1}\rangle \otimes |n\rangle_c$ , with  $N_1 = k$ ,  $N_0 = N + M - 2k - n$ , and  $N_{-1} = k - M + n$ , where  $N = N_1 + N_0 + N_{-1}$  and  $M = N_1 - N_{-1} + n$  are good quantum numbers in the absence of dissipation for initial  $M = 0$ . A near unit peak centered at the target twin-Fock state  $|10, 0; 0\rangle$  results even in the presence of dissipation. The inset of Fig. 3 (a) shows phase sensitivity of the prepared twin-Fock state when fed into a Ramsey interferometer [22, 70]. We find an entanglement-enhanced phase sensitivity  $[(\Delta\phi)_{\text{opt}}]$  at  $t_2$  of about 4.3 dB beyond the standard quantum limit (SQL)  $[(\Delta\phi)_{\text{SQL}} = 1/\sqrt{N}]$  at  $\kappa = 0$ , and the enhancement reduces to 1.6 dB at  $\kappa = 2|\tilde{c}|$ , implicating a favorable robustness of the present scheme for operational metrology gain. Photon loss tends to polarize atoms into  $M \leq 0$ , exemplified by the shifting distributions in Fig. 3 (b) out of the initial  $M = 0$  subspace from  $t = 0 \rightarrow t_1 \rightarrow t_2$ . Such atomic polarization mainly arise from the intrinsic asymmetry of our scheme by the presence of a significant QZS, which is not considered in early studies [41, 42, 56].

#### IV. CONCLUSIONS

In conclusion, we have proposed an efficient scheme for controlled spin-mixing dynamics based on tuning of both the spin-mixing rate and the competing QZS by changing pump lasers parameters. The tuned interaction occurs on a much faster time scale than inherent spin-exchange dynamics, and the synthesized spin-spin interaction as well as the effective QZS are essentially independent of the inherent atomic collision properties, therefore can be generalized to other atomic species, such as atoms with higher spins, alkali metals, or atomic mixtures. We hope this work will open the doors to more tunability in cold atom spin-spin interactions and their dynamics controls to enrich future experimental studies.

#### ACKNOWLEDGEMENTS

We acknowledge helpful discussions with Qi Liu and Xinwei Li. Numerical simulations are performed with QuTiP [86, 87].

#### Appendix A: Adiabatic elimination of excited states

Inside a large bias magnetic field, the inherent contact interactions between atoms are highly suppressed by the

quadratic Zeeman shift (QZS). The atom-cavity Hamiltonian becomes  $\hat{H} \approx \hat{H}_B + \omega_c \hat{c}^\dagger \hat{c} + \hat{H}_{\text{AL}}$ , with  $\hat{H}_B$  and  $\hat{H}_{\text{AL}}$  given in the main text. In the rotating frame defined by  $\hat{U} = \exp\{i(\hat{H}_B + \omega_c \hat{c}^\dagger \hat{c})t\}$ , the Hamiltonian in the new frame becomes  $\hat{H} = \hat{U} \hat{H} \hat{U}^\dagger + (i\partial_t \hat{U}) \hat{U}^\dagger$ , which is denoted by  $\hat{H}_1$  in the main text after rotating-wave approximation.

The large single- and two-photon detunings considered in this work ensures negligible occupation on atomic excited states, therefore adiabatic elimination of excited states is appropriate [69, 88].

We find after tedious calculations

$$\hat{H}_2 = \{[\eta_1 e^{-i(2q-\delta)t} + \eta_2 e^{i\delta t}] \hat{a}_0^\dagger \hat{a}_1 \hat{c}^\dagger + [\tilde{\eta}_1 e^{i\delta t} + \tilde{\eta}_2 e^{i(2q+\delta)t}] \hat{a}_{-1}^\dagger \hat{a}_0 \hat{c}^\dagger + \text{H.c.}\} + \hat{H}_{\text{Stark}}, \quad (\text{A1})$$

where  $\eta_{1,2}$  ( $\tilde{\eta}_{1,2}$ ) denote the cavity-assisted two-photon Raman coupling strengths defined by

$$\begin{aligned} \eta_1 &= g_1 \Omega_1 \left( \frac{1}{\Delta} + \frac{1}{\Delta + 2q - \delta} \right), \\ \eta_2 &= g_1 \Omega_2 \left( \frac{1}{\Delta + 2q} + \frac{1}{\Delta + 2q - \delta} \right), \\ \tilde{\eta}_1 &= g_2 \tilde{\Omega}_1 \left( \frac{1}{\Delta'} + \frac{1}{\Delta' - \delta} \right), \\ \tilde{\eta}_2 &= g_2 \tilde{\Omega}_2 \left( \frac{1}{\Delta' + 2q} + \frac{1}{\Delta' - \delta} \right). \end{aligned}$$

The Stark shift  $\hat{H}_{\text{Stark}} = [(\frac{\Omega_1^2}{\Delta} + \frac{\Omega_2^2}{\Delta + 2q}) \hat{a}_1^\dagger \hat{a}_1 + (\frac{g_1^2 \hat{c}^\dagger \hat{c}}{\Delta + 2q - \delta} + \frac{\tilde{\Omega}_1^2}{\Delta'} + \frac{\tilde{\Omega}_2^2}{\Delta' + 2q}) \hat{a}_0^\dagger \hat{a}_0 + (\frac{g_2^2 \hat{c}^\dagger \hat{c}}{\Delta' - \delta}) \hat{a}_{-1}^\dagger \hat{a}_{-1}] + [\Omega_1 \Omega_2 e^{i2qt} (\frac{1}{\Delta} + \frac{1}{\Delta + 2q}) \hat{a}_1^\dagger \hat{a}_1 + \tilde{\Omega}_1 \tilde{\Omega}_2 e^{i2qt} (\frac{1}{\Delta'} + \frac{1}{\Delta' + 2q}) \hat{a}_0^\dagger \hat{a}_0 + \text{h.c.}]$  induced by light fields is neglected in Eq.(3) of the main text for three ground-state levels. This term can be absorbed into the initial linear and quadratic Zeeman shifts in  $\hat{H}_B$ . In fact, it is much smaller than the Zeeman shifts for resonable sized bias magnetic field.

#### Appendix B: Time-independent Hamiltonian with Floquet-Magnus expansion

Here we use a simple approach to derive the effective Hamiltonian  $\hat{H}_{\text{eff}}$  given in the main text.

For the time periodic Hamiltonian,

$$\hat{H}_2(t) = [(\eta_1 e^{-i\omega t} + \eta_2 e^{i3\omega t}) \hat{a}_0^\dagger \hat{a}_1 \hat{c}^\dagger + (\eta_1 e^{i3\omega t} + \eta_2 e^{i7\omega t}) \hat{a}_{-1}^\dagger \hat{a}_0 \hat{c}^\dagger + \text{h.c.}], \quad (\text{B1})$$

with  $\omega = q/2$ , we can carry out the Floquet-Magnus expansion [72] and keep terms till the order of  $1/\omega$ . This yields the time-independent Hamiltonian,

$$\hat{H}_{\text{eff}} = \frac{1}{\omega} [\hat{V}_1, \hat{V}_{-1}] + \frac{1}{3\omega} [\hat{V}_3, \hat{V}_{-3}] + \frac{1}{7\omega} [\hat{V}_7, \hat{V}_{-7}], \quad (\text{B2})$$

where  $[\hat{A}, \hat{B}] = \hat{A}\hat{B} - \hat{B}\hat{A}$  being the commutator of operators  $\hat{A}$  and  $\hat{B}$ , and we have

$$\begin{aligned}\hat{V}_1 &= \eta_1 \hat{a}_1^\dagger \hat{a}_0 \hat{c}, & \hat{V}_3 &= \eta_2 \hat{a}_0^\dagger \hat{a}_1 \hat{c}^\dagger + \eta_1 \hat{a}_{-1}^\dagger \hat{a}_0 \hat{c}^\dagger, \\ \hat{V}_7 &= \eta_1 \hat{a}_{-1}^\dagger \hat{a}_0 \hat{c}^\dagger, & \hat{V}_m &= 0 \quad \text{for } m = \text{other integers.}\end{aligned}$$

It is straightforward to work out all the terms, and we find

$$\begin{aligned}[\hat{V}_1, \hat{V}_{-1}] &= \eta_1^2 (\hat{a}_1^\dagger \hat{a}_1 \hat{c} \hat{c}^\dagger - \hat{a}_0^\dagger \hat{a}_0 \hat{c}^\dagger \hat{c}) + \eta_1^2 \hat{a}_1^\dagger \hat{a}_0^\dagger \hat{a}_1 \hat{a}_0 [\hat{c}, \hat{c}^\dagger], \\ [\hat{V}_3, \hat{V}_{-3}] &= (\eta_1^2 \hat{a}_0^\dagger \hat{a}_{-1}^\dagger \hat{a}_{-1} \hat{a}_0 + \eta_2^2 \hat{a}_0^\dagger \hat{a}_1^\dagger \hat{a}_1 \hat{a}_0) \cdot [\hat{c}^\dagger, \hat{c}] \\ &\quad + \eta_1 \eta_2 (\hat{a}_0^\dagger \hat{a}_0^\dagger \hat{a}_1 \hat{a}_{-1} + \hat{a}_{-1}^\dagger \hat{a}_1^\dagger \hat{a}_0 \hat{a}_0) \cdot [\hat{c}^\dagger, \hat{c}] \\ &\quad + \eta_1^2 (\hat{a}_{-1}^\dagger \hat{a}_{-1} \hat{c}^\dagger \hat{c} - \hat{a}_0^\dagger \hat{a}_0 \hat{c} \hat{c}^\dagger) \\ &\quad + \eta_2^2 (\hat{a}_0^\dagger \hat{a}_0 \hat{c}^\dagger \hat{c} - \hat{a}_1^\dagger \hat{a}_1 \hat{c} \hat{c}^\dagger), \\ [V_7, V_{-7}] &= \eta_2^2 \hat{a}_{-1}^\dagger \hat{a}_0^\dagger \hat{a}_0 \hat{a}_{-1} \cdot [\hat{c}^\dagger, \hat{c}] \\ &\quad + \eta_2^2 (\hat{a}_{-1}^\dagger \hat{a}_{-1} \hat{c}^\dagger \hat{c} - \hat{a}_0^\dagger \hat{a}_0 \hat{c} \hat{c}^\dagger),\end{aligned}$$

which give

$$\begin{aligned}\hat{H}_{\text{eff}} \cdot \omega &= \left(\frac{1}{3}\eta_2^2 - \eta_1^2\right) \hat{a}_1^\dagger \hat{a}_0^\dagger \hat{a}_0 \hat{a}_1 \cdot [\hat{c}^\dagger, \hat{c}] \\ &\quad + \left(\frac{1}{3}\eta_1^2 + \frac{1}{7}\eta_2^2\right) \hat{a}_{-1}^\dagger \hat{a}_0^\dagger \hat{a}_0 \hat{a}_{-1} \cdot [\hat{c}^\dagger, \hat{c}] \\ &\quad + \frac{1}{3}\eta_1 \eta_2 (\hat{a}_0^\dagger \hat{a}_0^\dagger \hat{a}_1 \hat{a}_{-1} + \hat{a}_1^\dagger \hat{a}_{-1}^\dagger \hat{a}_0 \hat{a}_0) \cdot [\hat{c}^\dagger, \hat{c}] \\ &\quad + \left(\eta_1^2 - \frac{1}{3}\eta_2^2\right) (\hat{a}_1^\dagger \hat{a}_1 \hat{c} \hat{c}^\dagger - \hat{a}_0^\dagger \hat{a}_0 \hat{c}^\dagger \hat{c}) \\ &\quad + \left(\frac{1}{3}\eta_1^2 + \frac{1}{7}\eta_2^2\right) (\hat{a}_{-1}^\dagger \hat{a}_{-1} \hat{c}^\dagger \hat{c} - \hat{a}_0^\dagger \hat{a}_0 \hat{c} \hat{c}^\dagger).\end{aligned}$$

Substituting into  $\hat{c}^\dagger \hat{c} = 0$ ,  $\hat{c} \hat{c}^\dagger = 1$ , and taking  $\eta_2^2 = 3\eta_1^2 = 3\eta^2$ , the above reduces to the effective Hamiltonian,

$$\hat{H}_{\text{eff}} = \frac{\tilde{c}}{N} (\hat{a}_0^\dagger \hat{a}_0^\dagger \hat{a}_1 \hat{a}_{-1} + \text{h.c.}) - \tilde{q}_0 \hat{a}_{-1}^\dagger \hat{a}_0^\dagger \hat{a}_0 \hat{a}_{-1} - \tilde{q}_0 \hat{a}_0^\dagger \hat{a}_0, \quad (\text{B3})$$

where  $\tilde{c} = -\sqrt{3}N\eta^2/(3\omega)$  and  $\tilde{q}_0 = 16\eta^2/(21\omega) = 16\sqrt{3}|\tilde{c}|/(21N)$ . The residual density-density interaction term  $\propto \hat{a}_{-1}^\dagger \hat{a}_0^\dagger \hat{a}_0 \hat{a}_{-1}$  does not appreciably modify the spin-mixing dynamics.

Note that  $\tilde{c}$  may be positive if we choose an alternative cavity frequency condition to maintain an opposite sign of two-photon detuning, thereby rendering anti-ferromagnetic atomic spin-exchange interaction as in  $^{23}\text{Na}$  atoms.

### Appendix C: Tunability of the effective quadratic Zeeman shift

We consider  $(\omega_1, \omega_2) \rightarrow (\omega'_1, \omega'_2) = (\omega_1 + \tilde{q}/2, \omega_2 + 5\tilde{q}/2)$ , which gives  $\omega'_1 - \omega'_2 = 2(q - \tilde{q})$ , with  $|\tilde{q}| (\ll q)$  a small deviation from  $2q$ . The time-periodic Hamiltonian then takes the form

$$\begin{aligned}\hat{H}(t) &= \{[\eta_1 e^{-i(q/2 + \tilde{q}/2)t} + \eta_2 e^{i(3q/2 - 5\tilde{q}/2)t}] \hat{a}_0^\dagger \hat{a}_1 \hat{c}^\dagger \\ &\quad + [\eta_1 e^{i(3q/2 - \tilde{q}/2)t} + \eta_2 e^{i(7q/2 - 5\tilde{q}/2)t}] \hat{a}_{-1}^\dagger \hat{a}_0 \hat{c}^\dagger + \text{h.c.}\},\end{aligned}$$

we now change to work in the rotating frame defined by  $\hat{U}' = e^{i\tilde{q}\hat{a}_0^\dagger \hat{a}_0 t}$  and find

$$\begin{aligned}\tilde{H} &= \{[\eta_1 e^{-i(\frac{q}{2} - \frac{\tilde{q}}{2})t} + \eta_2 e^{i(\frac{3q}{2} - \frac{3\tilde{q}}{2})t}] \hat{a}_0^\dagger \hat{a}_1 \hat{c}^\dagger \\ &\quad + [\eta_1 e^{i(\frac{3q}{2} - \frac{3\tilde{q}}{2})t} + \eta_2 e^{i(\frac{7q}{2} - \frac{7\tilde{q}}{2})t}] \hat{a}_{-1}^\dagger \hat{a}_0 \hat{c}^\dagger + \text{h.c.}\} - \tilde{q} \hat{a}_0^\dagger \hat{a}_0.\end{aligned}$$

Following the same Floquet-Magnus approximation, we arrive at

$$\begin{aligned}\hat{H}_{\text{eff}} &= \frac{\tilde{c}}{N} (\hat{a}_0^\dagger \hat{a}_0^\dagger \hat{a}_{-1} \hat{a}_{-1} + \text{h.c.}) - \tilde{q}_0 \hat{a}_{-1}^\dagger \hat{a}_0^\dagger \hat{a}_0 \hat{a}_{-1} \\ &\quad - \tilde{q}_0 \hat{a}_0^\dagger \hat{a}_0 - \tilde{q} \hat{a}_0^\dagger \hat{a}_0,\end{aligned} \quad (\text{C1})$$

where  $\tilde{c} = -\sqrt{3}N\eta^2/(3\omega)$ ,  $\tilde{q}_0 = 16\eta^2/(21\omega)$ , and  $\omega = (q - \tilde{q})/2$ .

Therefore  $\tilde{q}$  indeed behaves as an effective quadratic Zeeman shift which can be easily tuned by changing the difference of two pump laser frequencies.

### Appendix D: Phase sensitivity

The optimal phase sensitivity [22]

$$(\Delta\phi)_{\text{opt}}^2 = \frac{V_{xz} + 2\Delta \hat{J}_x^2 \Delta \hat{J}_z^2}{4(\langle \hat{J}_x^2 \rangle - \langle \hat{J}_z^2 \rangle)^2}, \quad (\text{D1})$$

where  $V_{xz} = \langle (\hat{J}_x \hat{J}_z + \hat{J}_z \hat{J}_x)^2 \rangle + \langle \hat{J}_x^2 \hat{J}_z^2 + \hat{J}_z^2 \hat{J}_x^2 \rangle - 2\langle \hat{J}_z^2 \rangle \langle \hat{J}_x^2 \rangle$ ,  $\hat{J}_{i=x,y,z}$  is the collective spin operator for  $N$  spin-1/2. The expectation of observables are defined as  $\langle \hat{O} \rangle \equiv \text{Tr}(\hat{\rho} \hat{O})$  for density matrix  $\hat{\rho}$ .

- 
- [1] J. M. Raimond, M. Brune, and S. Haroche, Manipulating quantum entanglement with atoms and photons in a cavity, *Rev. Mod. Phys.* **73**, 565 (2001).  
[2] B. Morris, B. Yadin, M. Fadel, T. Zibold, P. Treutlein, and G. Adesso, Entanglement between identical particles is a useful and consistent resource, *Phys. Rev. X* **10**, 041012 (2020).

- [3] S. Sachdev, *Quantum Phase Transitions*, 2nd ed. (Cambridge University Press, 2011).  
[4] T.-L. Ho, Spinor Bose Condensates in Optical Traps, *Phys. Rev. Lett.* **81**, 742 (1998).  
[5] C. K. Law, H. Pu, and N. P. Bigelow, Quantum spins mixing in spinor Bose-Einstein condensates, *Phys. Rev. Lett.* **81**, 5257 (1998).

- [6] D. M. Stamper-Kurn, M. R. Andrews, A. P. Chikkatur, S. Inouye, H.-J. Miesner, J. Stenger, and W. Ketterle, Optical confinement of a bose-einstein condensate, *Phys. Rev. Lett.* **80**, 2027 (1998).
- [7] J. Stenger, S. Inouye, D. M. M. Stamper-Kurn, H.-J. Miesner, A. P. Chikkatur, and W. Ketterle, Spin domains in ground-state Bose–Einstein condensates, *Nature* **396**, 345 (1998).
- [8] M. S. Chang, C. D. Hamley, M. D. Barrett, J. A. Sauer, K. M. Fortier, W. Zhang, L. You, and M. S. Chapman, Observation of spinor dynamics in optically trapped  $^{87}\text{Rb}$  Bose-Einstein condensates, *Phys. Rev. Lett.* **92**, 140403 (2004).
- [9] M.-S. Chang, Q. Qin, W. Zhang, L. You, and M. S. Chapman, Coherent spinor dynamics in a spin-1 Bose condensate, *Nat. Phys.* **1**, 111 (2005).
- [10] L. E. Sadler, J. M. Higbie, S. R. Leslie, M. Vengalattore, and D. M. Stamper-Kurn, Spontaneous symmetry breaking in a quenched ferromagnetic spinor Bose–Einstein condensate, *Nature* **443**, 312 (2006).
- [11] S. Huh, K. Kim, K. Kwon, and J.-y. Choi, Observation of a strongly ferromagnetic spinor bose-einstein condensate, *Phys. Rev. Research* **2**, 033471 (2020).
- [12] X. Li, B. Zhu, X. He, F. Wang, M. Guo, Z.-F. Xu, S. Zhang, and D. Wang, Coherent heteronuclear spin dynamics in an ultracold spinor mixture, *Phys. Rev. Lett.* **114**, 255301 (2015).
- [13] F. Wang, X. Li, D. Xiong, and D. Wang, A double species  $^{23}\text{Na}$  and  $^{87}\text{Rb}$  bose–einstein condensate with tunable miscibility via an interspecies feshbach resonance, *J. Phys. B: At. Mol. Opt. Phys.* **49**, 015302 (2015).
- [14] L. Li, B. Zhu, B. Lu, S. Zhang, and D. Wang, Manipulation of heteronuclear spin dynamics with microwave and vector light shift, *Phys. Rev. A* **101**, 053611 (2020).
- [15] B. Lucke, M. Scherer, J. Kruse, L. Pezze, F. Deuretzbacher, P. Hyllus, O. Topic, J. Peise, W. Ertmer, J. Arlt, L. Santos, a. Smerzi, and C. Klempt, Twin Matter Waves for Interferometry Beyond the Classical Limit, *Science* **334**, 773 (2011).
- [16] C. D. Hamley, C. S. Gerving, T. M. Hoang, E. M. Bookjans, and M. S. Chapman, Spin-nematic squeezed vacuum in a quantum gas, *Nature Physics* **8**, 305 (2012).
- [17] W. Muessel, H. Strobel, D. Linnemann, D. B. Hume, and M. K. Oberthaler, Scalable spin squeezing for quantum-enhanced magnetometry with bose-einstein condensates, *Phys. Rev. Lett.* **113**, 103004 (2014).
- [18] T. Hoang, M. Anquez, B. Robbins, X. Yang, B. Land, C. Hamley, and M. Chapman, Parametric excitation and squeezing in a many-body spinor condensate, *Nat. Commun.* **7**, 11233 (2016).
- [19] J. Peise, I. Kruse, K. Lange, B. Lücke, L. Pezzè, J. Arlt, W. Ertmer, K. Hammerer, L. Santos, A. Smerzi, *et al.*, Satisfying the einstein–podolsky–rosen criterion with massive particles, *Nat. Commun.* **6**, 8984 (2015).
- [20] I. Kruse, K. Lange, J. Peise, B. Lücke, L. Pezzè, J. Arlt, W. Ertmer, C. Lisdat, L. Santos, A. Smerzi, and C. Klempt, Improvement of an atomic clock using squeezed vacuum, *Phys. Rev. Lett.* **117**, 143004 (2016).
- [21] D. Linnemann, H. Strobel, W. Muessel, J. Schulz, R. J. Lewis-Swan, K. V. Kheruntsyan, and M. K. Oberthaler, Quantum-enhanced sensing based on time reversal of nonlinear dynamics, *Phys. Rev. Lett.* **117**, 013001 (2016).
- [22] X.-Y. Luo, Y.-Q. Zou, L.-N. Wu, Q. Liu, M.-F. Han, M. K. Tey, and L. You, Deterministic entanglement generation from driving through quantum phase transitions, *Science* **355**, 620 (2017).
- [23] Y.-Q. Zou, L.-N. Wu, Q. Liu, X.-Y. Luo, S.-F. Guo, J.-H. Cao, M. K. Tey, and L. You, Beating the classical precision limit with spin-1 Dicke states of more than 10,000 atoms, *Proc. Natl. Acad. Sci.* **115**, 6381 (2018).
- [24] H. Saito, Y. Kawaguchi, and M. Ueda, Kibble-zurek mechanism in a quenched ferromagnetic bose-einstein condensate, *Phys. Rev. A* **76**, 043613 (2007).
- [25] E. Nicklas, M. Karl, M. Höfer, A. Johnson, W. Muesel, H. Strobel, J. Tomkovič, T. Gasenzer, and M. K. Oberthaler, Observation of scaling in the dynamics of a strongly quenched quantum gas, *Phys. Rev. Lett.* **115**, 245301 (2015).
- [26] M. Anquez, B. A. Robbins, H. M. Bharath, M. Boguslawski, T. M. Hoang, and M. S. Chapman, Quantum kibble-zurek mechanism in a spin-1 bose-einstein condensate, *Phys. Rev. Lett.* **116**, 155301 (2016).
- [27] M. Prüfer, P. Kunkel, H. Strobel, S. Lannig, D. Linnemann, C.-M. Schmied, J. Berges, T. Gasenzer, and M. K. Oberthaler, Observation of universal dynamics in a spinor bose gas far from equilibrium, *Nature* **563**, 217 (2018).
- [28] M. Xue, S. Yin, and L. You, Universal driven critical dynamics across a quantum phase transition in ferromagnetic spinor atomic bose-einstein condensates, *Phys. Rev. A* **98**, 013619 (2018).
- [29] C.-M. Schmied, M. Prüfer, M. K. Oberthaler, and T. Gasenzer, Bidirectional universal dynamics in a spinor bose gas close to a nonthermal fixed point, *Phys. Rev. A* **99**, 033611 (2019).
- [30] M. Greiner, O. Mandel, T. Esslinger, T. W. Hänsch, and I. Bloch, Quantum phase transition from a superfluid to a Mott insulator in a gas of ultracold atoms, *Nature* **415**, 39 (2002).
- [31] C. Chin, R. Grimm, P. Julienne, and E. Tiesinga, Feshbach resonances in ultracold gases, *Rev. Mod. Phys.* **82**, 1225 (2010).
- [32] S. Inouye, M. R. Andrews, J. Stenger, H. J. Miesner, D. M. Stamper-Kurn, and W. Ketterle, Observation of feshbach resonances in a bose–einstein condensate, *Nature* **392**, 151 (1998).
- [33] J. Stenger, S. Inouye, M. R. Andrews, H.-J. Miesner, D. M. Stamper-Kurn, and W. Ketterle, Strongly enhanced inelastic collisions in a bose-einstein condensate near feshbach resonances, *Phys. Rev. Lett.* **82**, 2422 (1999).
- [34] S. Blatt, T. L. Nicholson, B. J. Bloom, J. R. Williams, J. W. Thomsen, P. S. Julienne, and J. Ye, Measurement of optical feshbach resonances in an ideal gas, *Phys. Rev. Lett.* **107**, 073202 (2011).
- [35] H. Wu and J. E. Thomas, Optical control of feshbach resonances in fermi gases using molecular dark states, *Phys. Rev. Lett.* **108**, 010401 (2012).
- [36] K. T. Kapale, G. S. Agarwal, and M. O. Scully, Cavity-mediated long-range interaction for fast multiqubit quantum logic operations, *Phys. Rev. A* **72**, 052304 (2005).
- [37] R. Mottl, F. Brennecke, K. Baumann, R. Landig, T. Donner, and T. Esslinger, Roton-type mode softening in a quantum gas with cavity-mediated long-range interactions, *Science* **336**, 1570 (2012).
- [38] C. Aron, M. Kulkarni, and H. E. Türeci, Photon-mediated interactions: A scalable tool to create and sustain entangled states of  $n$  atoms, *Phys. Rev. X* **6**, 011032 (2016).

- (2016).
- [39] C.-L. Hung, A. González-Tudela, J. I. Cirac, and H. J. Kimble, Quantum spin dynamics with pairwise-tunable, long-range interactions, *Proc. Natl. Acad. Sci.* **113**, E4946 (2016).
- [40] Y.-C. Zhang, X.-F. Zhou, X. Zhou, G.-C. Guo, and Z.-W. Zhou, Cavity-Assisted Single-Mode and Two-Mode Spin-Squeezed States via Phase-Locked Atom-Photon Coupling, *Phys. Rev. Lett.* **118**, 083604 (2017).
- [41] S. J. Masson, M. D. Barrett, and S. Parkins, Cavity QED Engineering of Spin Dynamics and Squeezing in a Spinor Gas, *Phys. Rev. Lett.* **119**, 213601 (2017).
- [42] E. J. Davis, G. Bentsen, L. Homeier, T. Li, and M. H. Schleier-Smith, Photon-mediated spin-exchange dynamics of spin-1 atoms, *Phys. Rev. Lett.* **122**, 010405 (2019).
- [43] F. Mivehvar, H. Ritsch, and F. Piazza, Cavity-quantum-electrodynamical toolbox for quantum magnetism, *Phys. Rev. Lett.* **122**, 113603 (2019).
- [44] D. Porras and J. I. Cirac, Effective quantum spin systems with trapped ions, *Phys. Rev. Lett.* **92**, 207901 (2004).
- [45] K. Kim, M. S. Chang, S. Korenblit, R. Islam, E. E. Edwards, J. K. Freericks, G. Lin, L. Duan, and C. Monroe, Quantum simulation of frustrated ising spins with trapped ions, *Nature* **465**, 590 (2010).
- [46] J. W. Britton, B. C. Sawyer, A. C. Keith, C. C. J. Wang, J. K. Freericks, H. Uys, M. J. Biercuk, and J. J. Bollinger, Engineered two-dimensional Ising interactions in a trapped-ion quantum simulator with hundreds of spins, *Nature* **484**, 489 (2012).
- [47] D. A. Golter, T. Oo, M. Amezcua, K. A. Stewart, and H. Wang, Optomechanical quantum control of a nitrogen-vacancy center in diamond, *Phys. Rev. Lett.* **116**, 143602 (2016).
- [48] P.-B. Li, Y. Zhou, W.-B. Gao, and F. Nori, Enhancing spin-phonon and spin-spin interactions using linear resources in a hybrid quantum system, *Phys. Rev. Lett.* **125**, 153602 (2020).
- [49] I. Bouchoule and K. Mølmer, Spin squeezing of atoms by the dipole interaction in virtually excited rydberg states, *Phys. Rev. A* **65**, 041803 (2002).
- [50] N. Henkel, R. Nath, and T. Pohl, Three-dimensional roton excitations and supersolid formation in rydberg-excited bose-einstein condensates, *Phys. Rev. Lett.* **104**, 195302 (2010).
- [51] A. W. Glaetzle, M. Dalmonte, R. Nath, C. Gross, I. Bloch, and P. Zoller, Designing frustrated quantum magnets with laser-dressed rydberg atoms, *Phys. Rev. Lett.* **114**, 173002 (2015).
- [52] P. Schauß, J. Zeiher, T. Fukuhara, S. Hild, M. Cheneau, T. Macrì, T. Pohl, I. Bloch, and C. Gross, Crystallization in ising quantum magnets, *Science* **347**, 1455 (2015).
- [53] J. Zeiher, J.-y. Choi, A. Rubio-Abadal, T. Pohl, R. van Bijnen, I. Bloch, and C. Gross, Coherent many-body spin dynamics in a long-range interacting ising chain, *Phys. Rev. X* **7**, 041063 (2017).
- [54] F. Yang, Y.-C. Liu, and L. You, Atom-photon spin-exchange collisions mediated by rydberg dressing, *Phys. Rev. Lett.* **125**, 143601 (2020).
- [55] V. Borish, O. Marković, J. A. Hines, S. V. Rajagopal, and M. Schleier-Smith, Transverse-field ising dynamics in a rydberg-dressed atomic gas, *Phys. Rev. Lett.* **124**, 063601 (2020).
- [56] A. Periwal, E. S. Cooper, P. Kunkel, J. F. Wienand, E. J. Davis, and M. Schleier-Smith, Programmable interactions and emergent geometry in an array of atom clouds, *Nature* **600**, 630 (2021).
- [57] K. Murata, H. Saito, and M. Ueda, Broken-axisymmetry phase of a spin-1 ferromagnetic Bose-Einstein condensate, *Phys. Rev. A* **75**, 013607 (2007).
- [58] S. Uchino, M. Kobayashi, and M. Ueda, Bogoliubov theory and lee-huang-yang corrections in spin-1 and spin-2 bose-einstein condensates in the presence of the quadratic zeeman effect, *Phys. Rev. A* **81**, 063632 (2010).
- [59] L. Pezzè, M. Gessner, P. Feldmann, C. Klempt, L. Santos, and A. Smerzi, Heralded generation of macroscopic superposition states in a spinor bose-einstein condensate, *Phys. Rev. Lett.* **123**, 260403 (2019).
- [60] T. Elsässer, B. Nagorny, and A. Hemmerich, Optical bistability and collective behavior of atoms trapped in a high-q ring cavity, *Phys. Rev. A* **69**, 033403 (2004).
- [61] F. Brennecke, T. Donner, S. Ritter, T. Bourdel, M. Köhl, and T. Esslinger, Cavity QED with a Bose-Einstein condensate, *Nature* **450**, 268 (2007).
- [62] L. Zhao, J. Jiang, T. Tang, M. Webb, and Y. Liu, Antiferromagnetic Spinor Condensates in a Two-Dimensional Optical Lattice, *Phys. Rev. Lett.* **114**, 225302 (2015).
- [63] E. M. Bookjans, C. D. Hamley, and M. S. Chapman, Strong quantum spin correlations observed in atomic spin mixing, *Phys. Rev. Lett.* **107**, 210406 (2011).
- [64] T. M. Hoang, C. S. Gerving, B. J. Land, M. Anquez, C. D. Hamley, and M. S. Chapman, Dynamic Stabilization of a Quantum Many-Body Spin System, *Phys. Rev. Lett.* **111**, 090403 (2013).
- [65] B. Evrard, A. Qu, J. Dalibard, and F. Gerbier, From many-body oscillations to thermalization in an isolated spinor gas, *Phys. Rev. Lett.* **126**, 063401 (2021).
- [66] H. Pu, C. K. Law, S. Raghavan, J. H. Eberly, and N. P. Bigelow, Spin-mixing dynamics of a spinor bose-einstein condensate, *Phys. Rev. A* **60**, 1463 (1999).
- [67] A. T. Black, E. Gomez, L. D. Turner, S. Jung, and P. D. Lett, Spinor dynamics in an antiferromagnetic spin-1 condensate, *Phys. Rev. Lett.* **99**, 070403 (2007).
- [68] Y. Liu, S. Jung, S. E. Maxwell, L. D. Turner, E. Tiesinga, and P. D. Lett, Quantum phase transitions and continuous observation of spinor dynamics in an antiferromagnetic condensate, *Phys. Rev. Lett.* **102**, 125301 (2009).
- [69] H. J. Carmichael, *Statistical methods in quantum optics 1: master equations and Fokker-Planck equations*, Vol. 1 (Springer Science & Business Media, 1999).
- [70] See the Supplemental Material.
- [71] R. Mottl, *Roton-type mode softening in a dissipative quantum many-body system with cavity-mediated long-range interactions*, Ph.D. thesis, ETH Zurich (2014).
- [72] A. Eckardt, Colloquium: Atomic quantum gases in periodically driven optical lattices, *Rev. Mod. Phys.* **89**, 011004 (2017).
- [73] S.-B. Zheng and G.-C. Guo, Efficient scheme for two-atom entanglement and quantum information processing in cavity qed, *Phys. Rev. Lett.* **85**, 2392 (2000).
- [74] C. Groiseau, A. E. J. Elliott, S. J. Masson, and S. Parkins, Proposal for a deterministic single-atom source of quasisuperradiant  $n$ -photon pulses, *Phys. Rev. Lett.* **127**, 033602 (2021).
- [75] L. Zhao, J. Jiang, T. Tang, M. Webb, and Y. Liu, Dynamics in spinor condensates tuned by a microwave dressing field, *Phys. Rev. A* **89**, 023608 (2014).
- [76] H. Sun, P. Xu, H. Pu, and W. Zhang, Efficient generation of many-body singlet states of spin-1 bosons in optical



- superlattices, *Phys. Rev. A* **95**, 063624 (2017).
- [77] S. J. Masson and S. Parkins, Preparing the spin-singlet state of a spinor gas in an optical cavity, *Phys. Rev. A* **99**, 013819 (2019).
- [78] A. Qu, B. Evrard, J. Dalibard, and F. Gerbier, Probing spin correlations in a bose-einstein condensate near the single-atom level, *Phys. Rev. Lett.* **125**, 033401 (2020).
- [79] S.-F. Guo, F. Chen, Q. Liu, M. Xue, J.-J. Chen, J.-H. Cao, T.-W. Mao, M. K. Tey, and L. You, Faster state preparation across quantum phase transition assisted by reinforcement learning, *Phys. Rev. Lett.* **126**, 060401 (2021).
- [80] K. Baumann, C. Guerlin, F. Brennecke, and T. Esslinger, Dicke quantum phase transition with a superfluid gas in an optical cavity, *Nature* **464**, 1301 (2010).
- [81] R. Landig, L. Hruby, N. Dogra, M. Landini, R. Mottl, T. Donner, and T. Esslinger, Quantum phases from competing short- and long-range interactions in an optical lattice, *Nature* **532**, 476 (2016).
- [82] J. Leonard, A. Morales, P. Zupancic, T. Esslinger, and T. Donner, Supersolid formation in a quantum gas breaking a continuous translational symmetry, *Nature* **543**, 87 (2017).
- [83] H. Keßler, J. Klinder, M. Wolke, and A. Hemmerich, Steering Matter Wave Superradiance with an Ultranarrow-Band Optical Cavity, *Phys. Rev. Lett.* **113**, 070404 (2014).
- [84] J. Klinder, H. Keßler, M. Wolke, L. Mathey, and A. Hemmerich, Dynamical phase transition in the open dicke model, *Proc. Natl. Acad. Sci.* **112**, 3290 (2015).
- [85] A. Georgakopoulos, *Modeling and Creating Cavity Rydberg Polaritons for Achieving Strongly Correlated Photonic Materials* (The University of Chicago, 2018).
- [86] J. Johansson, P. Nation, and F. Nori, Qutip: An open-source python framework for the dynamics of open quantum systems, *Comput. Phys. Commun.* **183**, 1760 (2012).
- [87] J. Johansson, P. Nation, and F. Nori, Qutip 2: A python framework for the dynamics of open quantum systems, *Comput. Phys. Commun.* **184**, 1234 (2013).
- [88] F. Reiter and A. S. Sørensen, Effective operator formalism for open quantum systems, *Phys. Rev. A* **85**, 032111 (2012).